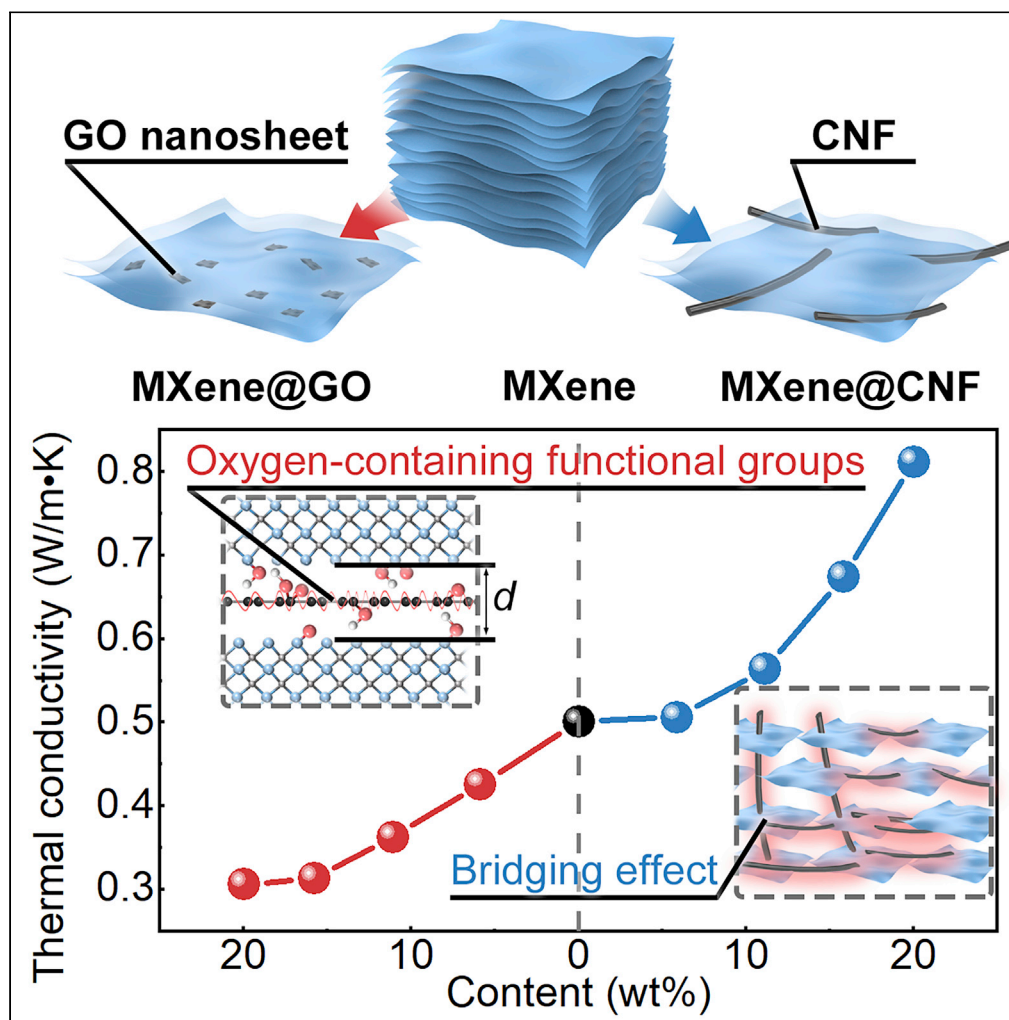Article

Synergistical thermal modulation function of 2D Ti$_3$C$_2$ MXene composite nanosheets via interfacial structure modification

Yuxin Ouyang, Lin Qiu, Yangyang Bai, Wei Yu, Yanhui Feng

qiulin@ustb.edu.cn (L.Q.)
yhfeng@me.ustb.edu.cn (Y.F.)

Highlights

MXene nanosheet with nanometer lateral dimensions was produced by etching

Design and application of the flexible thermosensor-based third harmonic method

Thermal barrier effect of interfacial oxygen-containing functional groups

Thermal bridging effect of carbon nanofibers across multiple MXene nanosheets

Article

Synergistical thermal modulation function of 2D Ti$_3$C$_2$ MXene composite nanosheets via interfacial structure modification

Yuxin Ouyang,[1,4] Lin Qiu,[1,2,4,5,*] Yangyang Bai,[1] Wei Yu,[3] and Yanhui Feng[1,2,*]

SUMMARY

MXene demonstrates high in-plane thermal transport merit as an emerging two-dimensional material, but its out-of-plane thermal transport did not fully explore. Here Ti$_3$C$_2$ MXene nanosheets with either GO or CNF fillers were fabricated by using the vacuum-assisted filtration method. It was found that the addition of GO and CNF enlarged the interlayer spacing of the MXene layers, bringing about the opportunity for changeable spatial configuration of fillers and the thermal regulation function. If the GO nanosheets were interspersed parallel to the MXene layers, strong interference of increasing oxygen-containing functional group suppresses the out-of-plane thermal transport, resulting in the thermal conductivity decreasing from 0.5 W/(m·K) to 0.31 W/(m·K) for 20 wt% GO addition. Moreover, CNFs formed out-of-plane protruding on the surface of MXene nanosheets, resulting in the thermal conductivity increasing to 0.81 W/(m·K) for 20 wt% CNF addition. This discovery navigates how to prepare MXene composites with customized thermal properties.

INTRODUCTION

As electronic devices become smaller and more integrated, thermal management has become a vital issue in product design, production, and application in micro- and nano-electronics. To handle this, the nano thermal interface material (nTIM) has been developing which plays a role in assisting the heat dissipation at the device-heat sink interfaces and interlayer interfaces within the device. A qualified nTIM needs to possess excellent thermal conductivity either along the plane or out of the plane. Conventional nTIM are supposed to have ultra-high out-of-plane thermal conductivity which is conductive to heat conduction from the device to the heat sink, while a recently concept holds that nTIM with good in-plane thermal conductivity is also welcome because heat can be rapidly dissipated along the plane direction. Hence, two-dimensional (2D) materials have attracted wide attention owing to their anisotropic thermal transport characteristics (Butler et al., 2013). MXene emerges as a new 2D material which is generally obtained by etching the A-layer of MAX materials. Here M denotes a transition metal, A denotes an element of group IIIA and IVA metal, and X denotes C and/or N element (Naguib et al., 2011). The remaining MX layer forms a 2D material similar to graphene. After etching A-layer atoms, the top and bottom surfaces of the MX layer are replaced by functional groups (-O-, -OH, -F, -Cl), which makes MXene have excellent performance in the fields of energy storage, adsorption, and photothermal conversion (Hu et al., 2013; Lukatskaya Maria et al., 2013; Naguib et al., 2014). As a member of 2D materials, the superior in-plane thermal conductivity of ~2.84 W/(m·K) for pure MXene is reported (Chen et al., 2018). The composite of MXene with various materials can further improve its in-plane thermal conductivity dozens of times, but the out-of-plane thermal conductivity of these materials is below 0.50 W/(m·K) (Gao et al., 2021; Jiao et al., 2021a, 2021b), which greatly inhibits the design of MXene as nTIM. Moreover, the out-plane thermal transport characteristics of MXene have not yet been fully understood.

To explore the thermal properties of MXene family materials, a new measurement technique is urgently needed. The well-known 3ω method is verified to be useful for the thermal measurement of 2D materials (Cahill and Pohl, 1987; Qiu et al., 2013, 2018, 2021a, 2021b). The upgraded form of the 3ω method, that is the freestanding thermosensor-based 3ω method enables the 2D nanosheets can be noninvasively measured (Qiu et al., 2011), which significantly retains the integrity of the 2D materials. Here Ti$_3$C$_2$ MXene nanosheets with either carbon nanofibers or graphene oxide fillers were fabricated by etching Ti$_3$AlC$_2$ with
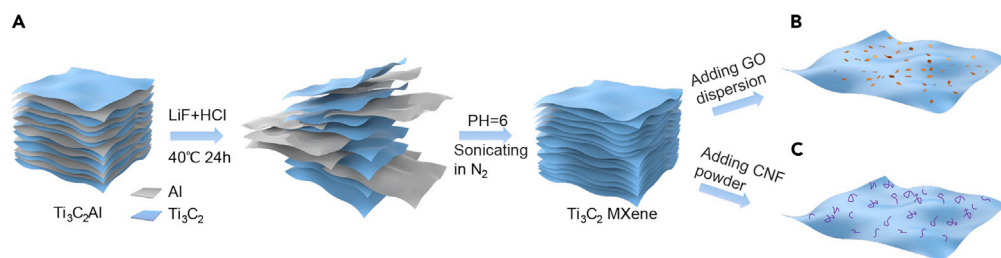
Figure 1. Schematic diagram of the preparation procedure

(A) Hydrochloric acid and fluoride salt mixed solution etching to produce Ti_3C_2 MXene, and (B) GO nanosheets are dispersed on the surface of MXene nanosheets through the similar compatibility of oxygen-containing functional groups on the surface.

(C) CNF dispersed between MXene nanosheets to build network structure.

LiF and HCl (Figure 1). The thermal properties of MXene and its composite nanosheets were measured using the freestanding thermosensor-based 3ω method (Figure 2). Detailed analysis of their thermal transport mechanism was carried out which could guide the customized design of MXene materials.

RESULTS AND DISCUSSION

Microstructure of MXene films and its composite films

After sonication, the lateral sizes of MXene nanosheets are found to be within 50-200 nm. The TEM micrographs of MXene powders are shown in Figure 3. It can be seen that a piece of MXene sheet with a characteristic diameter of approximately 70 nm usually renders an ultra-thin few-layer morphology (Figure 3A). The smaller size is beneficial for mixing with other materials to build a thermally conductive network along the out-of-plane direction. However, the smaller contact area greatly reduces the in-plane stiffness of the pure MXene films, which makes the strength of the MXene films much lower than that of those prepared from micron-scale lateral size (Luo et al., 2020; Wang et al., 2021). The layer spacing of the two nanosheets is about 1.1 nm (Figure 3B). Under the high-resolution image, the atomic arrangement of MXene is hexagonal, which is the same as that of the parent MAX phase. The lattice parameter $D_{(101)} = 0.21$ nm (Figure 3C). The discrete diffraction pattern shows the clear crystal structure of MXene, indicating that the sample has been successfully prepared (Figure 3D).

SEM micrographs indicate that the MXene nanosheets are stacked together with flat surfaces, which are connected with each other through van der Waals forces to form a multilayer sheet stacking structure (Figures 4A and 4B). There are fragments on the MXene@graphene oxide (MXene@GO) film surface (Figures 4C and 4D) owing to the interpenetration of GO and MXene nanosheets; however, the size of GO sheets is more petite than MXene and the surface flatness has changed slightly. As to the MXene@carbon nanofibers (MXene@CNF) film, in addition to the layered structure of the main body like the MXene film, there are prominent surface protrusions caused by vertically interspersed CNF on its surface (Figures 4E and 4F), which may affect the MXene layer spacing and film stiffness. The elemental composition and ratio of the prepared films were obtained by energy dispersive spectroscopy (EDS) scanning (Table 1 exhibits elemental comparison of the pristine and 20 wt% filler content). It is demonstrated that the main components of the MXene samples prepared from the precursor are $Ti_3C_2T_x$, where T represents the oxygen-containing functional group and a small amount of fluorine-containing functional groups. Moreover, the content of Al below 1% also proves the better purity of MXene (Na comes from L-Ascorbic acid sodium). After the addition of GO and CNF, the content of the C element in the composite films increased and the content of the O element decreased. However, owing to the presence of oxygen-containing functional groups on the surface of GO, the decrease in the proportion of oxygen elements in MXene@GO films is relatively low. It is to be noted that the proportion of Na element is greatly reduced after adding the fillers, which is hard to be detected by the EDS method.

Structural effect of MXene purity and doping

The XRD patterns of the three films are shown in Figure 5A. The prominent (002) peak near 6.5° is the most significant characteristic peak of Ti_3C_2, consistent with previous reports (Murugan et al., 2021). Another evidence confirming the synthesis of MXene is the existence of other peaks, such as (004) and (008) peaks. The
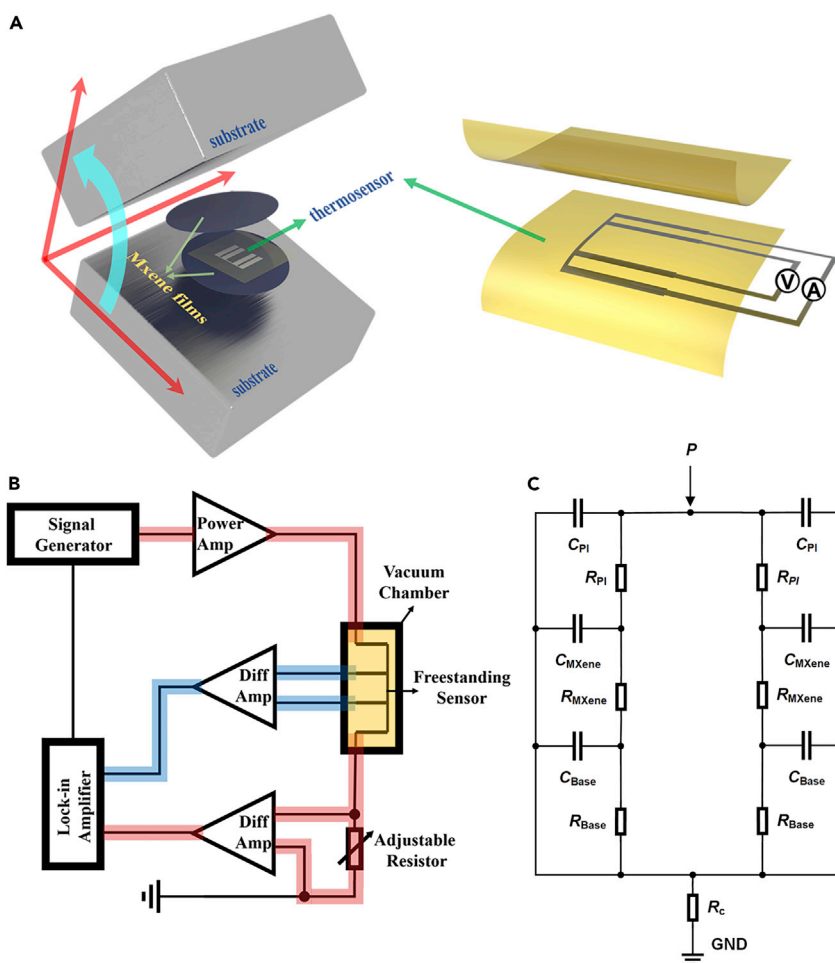
Figure 2. Schematic diagram of the thermophysical property measuring system
(A) Schematic diagram of the composition of the freestanding thermosensor, and (B) experimental system for the freestanding thermosensor-based 3ω technique.
(C) Thermal resistance network diagram of the test structure.

characteristic peak of the precursor Ti_3AlC_2 is substantially weakened, indicating that the reaction is relatively complete and the relatively pure MXene nanosheets were prepared. For the MXene@GO and MXene@CNF samples, the (002) peak position shifted slightly to the left, and the characteristic peak became narrower and higher, which indicates that the layer spacing of MXene changes after adding other fillers. According to the Bragg equation, the spacing is calculated to be 1.35 nm (MXene), 1.38 nm (MXene@GO), and 1.42 nm (MXene@CNF), respectively. This result shows that the addition of GO and CNF inhibits the self-accumulation of MXene and thus increases the layer spacing.

Raman spectra of the three samples also exhibit remarkable differences (Figure 5B). The characteristic peaks of MXene mainly appear at 180-780 cm^{-1}. The peaks at I correspond to the out-of-plane vibration of the A_{1g} symmetry of Ti and C atoms. The vibrations at II and III are assigned to the in-plane (E_g) vibrations of surface functional groups attached to Ti atoms. The IV region and V peak represent the carbon vibrations of E_g and A_{1g} (Sarycheva and Gogotsi, 2020), respectively. In the MXene@GO films, the significant D peak and G peak can be observed, and the ratio of I_D/I_G is 0.97, while the redshift of the I peak may be caused by the slight oxidation of the surface during the preparation process.

Thermal conductivity comparison among 2D thin films

The experimental temperature rise data of the freestanding thermosensor-based 3ω technique are shown in Figure 6. When the frequency is above 1 Hz, the temperature rise of different materials is consistent
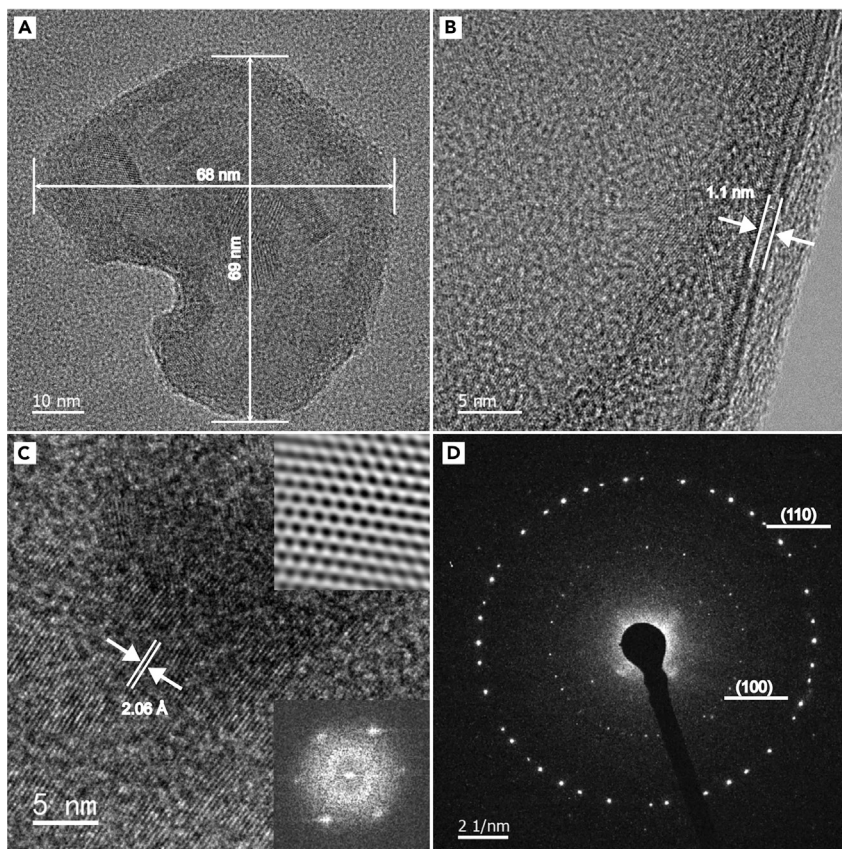
Figure 3. TEM micrographs of the prepared MXene nanosheet
(A) Microscopic morphology of a few layers of graphene nanosheets.
(B) Microscopic morphology of a piece of double-layer MXene nanosheet.
(C) High-resolution TEM images of MXene along with Fast Fourier transform (bottom right) and Inverse Fast Fourier Transform (top right) images.
(D) Selected area electron diffraction pattern of the MXene nanosheet.

owing to the thermal wave has not penetrated through the polyimide film of the thermosensor. With the frequency decreasing gradually, the difference in the temperature rise among the samples with different concentrations of fillers becomes remarkable below 0.3 Hz. The out-of-plane thermal conductivity of the nanosheets is shown in Table 2. The obtained thermal conductivity of the pure MXene nanosheet is 0.50 W/m·K.

Filling of high thermal conductivity materials can improve the thermal properties of raw materials, while two different dopants (GO and CNF) exhibit two different thermal conductivity phenomena. With the increase of GO content, the thermal conductivity of MXene@GO films showed a nonlinear decreasing trend (Figure 6C), reaching 0.31 W/(m·K) at the 20 wt%. Whereas the MXene@CNF films showed the opposite trend (Figure 6D), increasing to 0.81 W/m·K at the 20 wt%. This is mainly derived from the interesting interaction of two nanomaterials on the interfacial thermal transport of MXene nanosheets.

According to the XRD characterization results, the layer spacing expansion effect is attributed to doping, even if it is not the only cause of thermal conductivity changes in composite films. The microstructure of composite films (Figure 4) indicates that GO fillers are widely attached to the surface and interface of MXene with the help of a similar nature of their functional groups (Table 1), which helps increase the strength of the films (Figure 7). However, the functional groups between GO and MXene have multiple effects on phonon transport. For the interior of GO, the content of functional groups on the surface increases under the contact interaction, and the stretching effect on the C-C bonds is obvious, resulting in
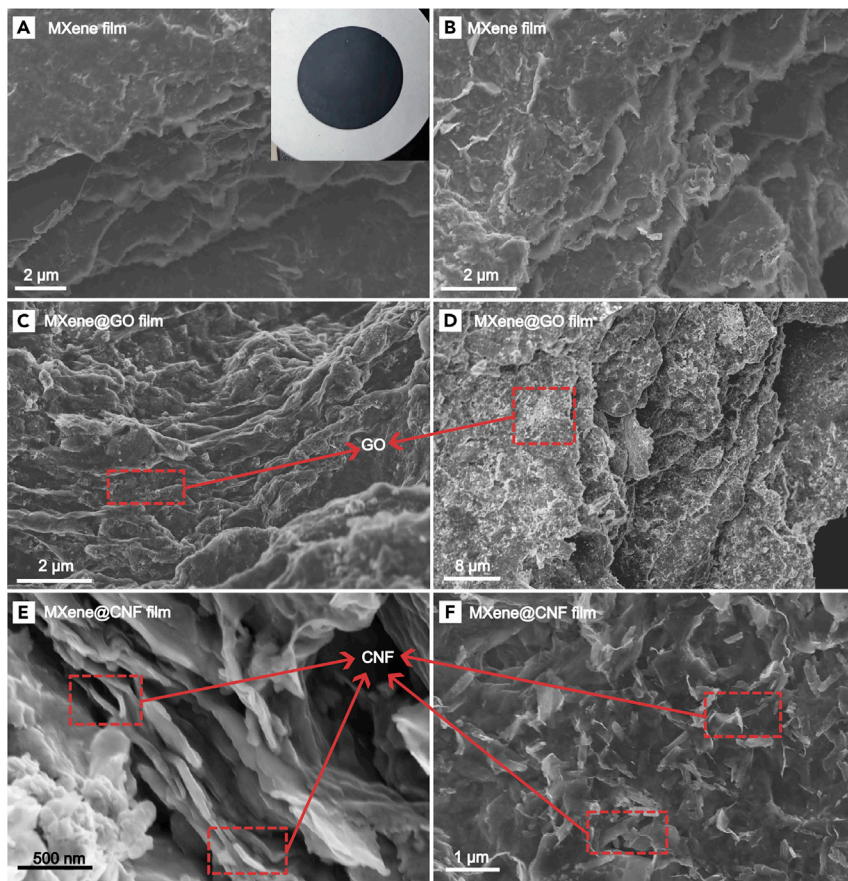
Figure 4. SEM micrographs of pure MXene, MXene@Go, and MXene@CNT nanosheets
(A and B) Microscopic structure of MXene nanosheets, inset: a piece of real MXene film after extraction, (C and D) Microscopic structure of MXene@GO film with nanosheets on the surface, (E and F) Microscopic structure of MXene@CNF film with a normal convexity of the surface.

widespread small ripples on the carbon network (Figure 7). This displacement of C atoms weakens the in-plane thermal transport capability (Sun et al., 2018; Wang et al., 2013). Similarly, more functional groups further increase the interfacial spacing though the short-range and long-range interactions among atoms were improved (Liang et al., 2013), resulting in more intense phonon heat dissipation and increasing the interfacial thermal resistance between nanosheets (Wei et al., 2011). Interestingly, with the increased

Table 1. Elemental content of MXene films and its composite films with 20 wt% filler content

Element	MXene		MXene@GO		MXene@CNF	
	wt%[a]	at%[b]	wt%	at%	wt%	at%
C	6.43	15.90	12.04	28.63	13.57	31.70
O	15.34	28.50	11.21	20.01	8.97	15.73
F	5.51	8.62	5.06	7.61	5.91	8.59
Na	0.82	1.06	≈0	≈0	≈0	≈0
Cl	3.97	3.32	4.28	3.45	4.47	3.53
Ti	67.05	41.62	67.17	40.05	66.14	39.39
Al	0.89	0.98	0.24	0.25	0.76	0.83

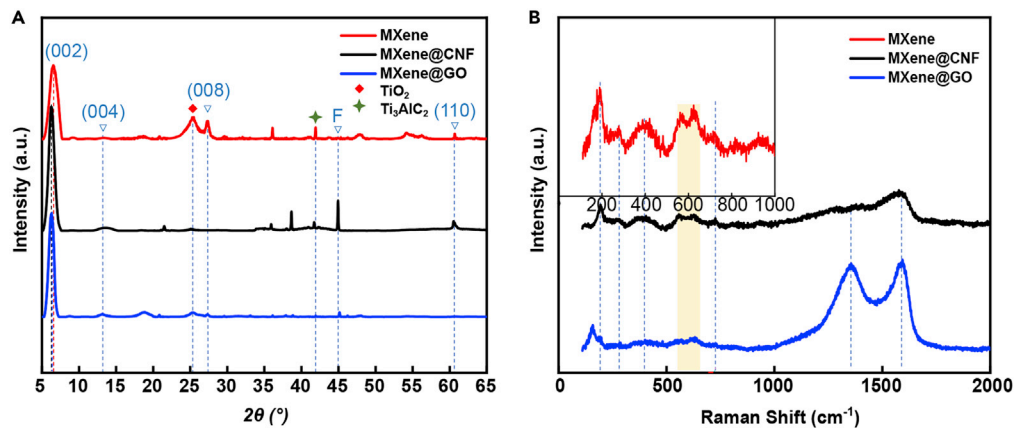[a]Weight percentage.
[b]Atomic percentage.

Figure 5. Light-wave characterization of the prepared MXene and composites films
(A) XRD patterns and (B) Raman spectra.

addition of GO, the decreasing trend of the thermal conductivity for the composite films flattened. This may be the reason for the contact area limitations (Figures 4C and 4D) and the decreasingly total content of functional groups (Table 1).

The doping of CNF produces different interactions. Owing to the pure C atomic structure, the connection between CNF and MXene is mainly through van der Waals force. Larger interfacial spacing is characterized
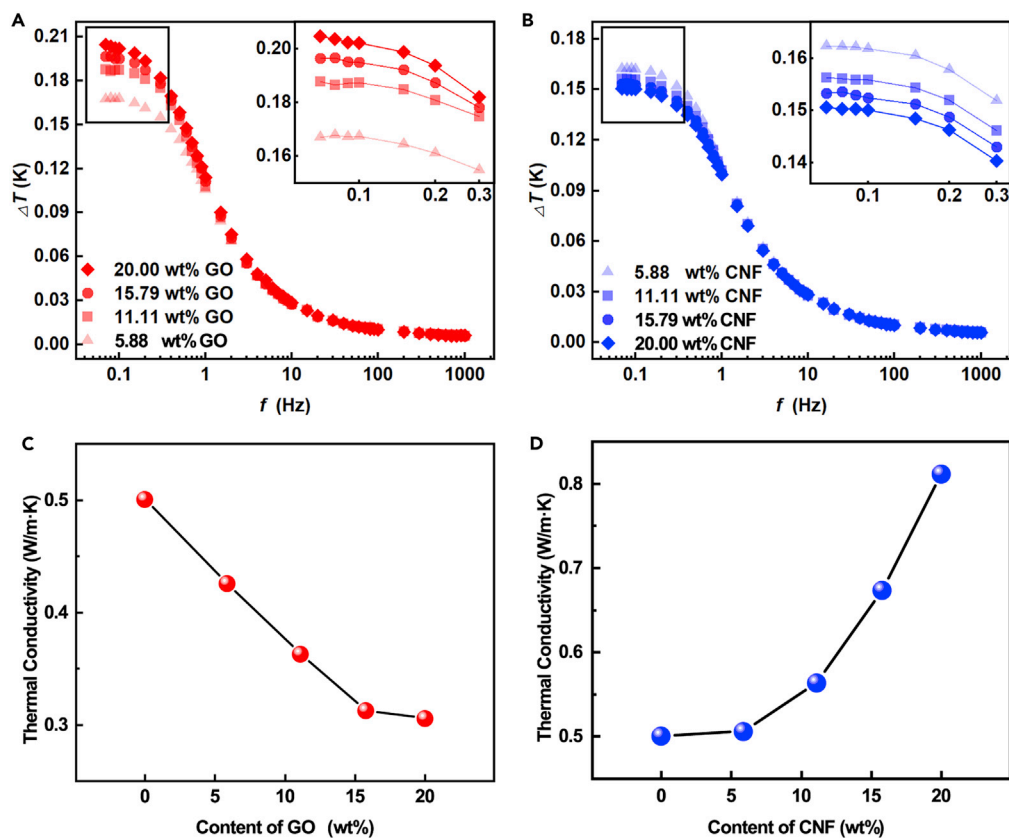

Figure 6. Experimental temperature rise data of freestanding thermosensor
(A) MXene@GO and (B) MXene@CNF nanosheets with different additions, and the obtained thermal conductivity for (C) MXene@GO and (D) MXene@CNF nanosheets.
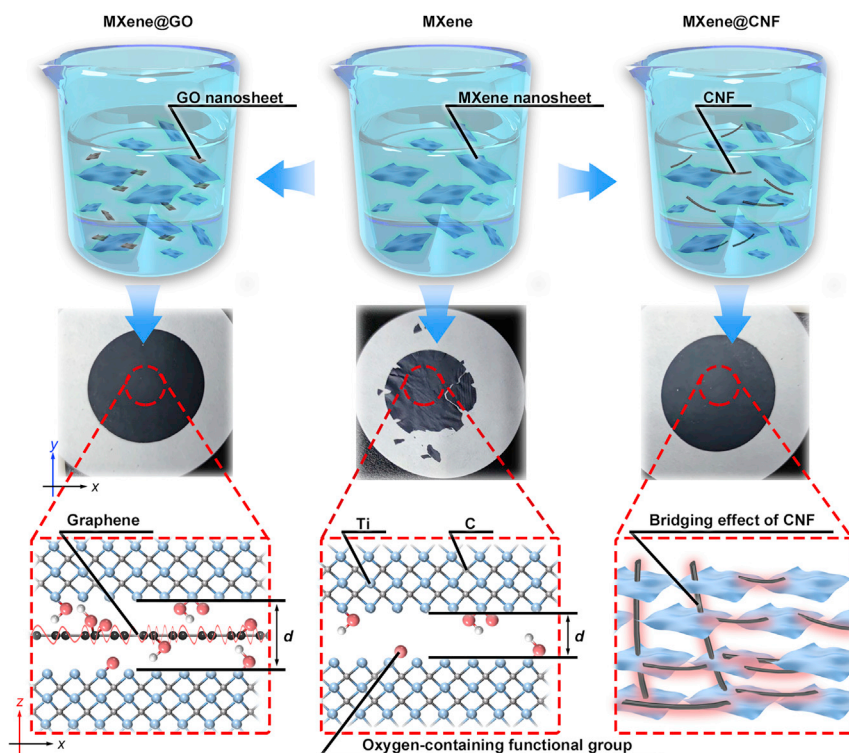
Figure 7. Schematic diagram of the heat transport mechanism for the preparation of thin films
From top to bottom, it is shown as the mixing process of MXene nanosheets, GO nanosheets, and CNF, the prepared film material (owing to the poor mechanical properties of MXene, the pure MXene film is broken), as well as the interaction between atoms of different materials and the influence of thermal transport.

by XRD, but the more prominent aspect ratio characteristics make CNFs exhibit a structural synergistic merit in MXene. Figures 4E and 4F demonstrate randomly oriented networks interspersed between nanosheets, which induces the bridging effect (Figure 7) that can enhance the mechanical properties of composite films (Jiao et al., 2021a, 2021b) and create a thermal transfer path between nanosheets (Badakhsh et al., 2019; Che et al., 2017, 2018). Moreover, the order of addition in the preparation (adding CNFs in dispersed MXene nanosheets) also reduces the phenomenon of CNFs agglomeration (Xiao et al., 2016). Thus, the adding CNF could improve the thermal conductivity of MXene composite film (Figure 6D).

Conclusion

In this study, MXene nanosheets were prepared by using the etching method. MXene nanosheets and their composites with CNF and GO addition were prepared, respectively. The out-of-plane thermal conductivity of the MXene nanosheets was obtained to be 0.50 W/(m·K) via the freestanding thermosensor-based 3ω method. The thermal conductivity of the MXene@GO nanosheets only decreases to 0.31 W/(m·K) owing

Table 2. The out-of-plane thermal conductivity of MXene nanosheet and its composite materials

MXene	MXene@GO		MXene@CNF	
Thermal conductivity W/(m·K)	Content of GO (wt%)	Thermal conductivity W/(m·K)	Content of CNF (wt%)	Thermal conductivity W/(m·K)
0.50	5.88	0.43	5.88	0.51
	11.11	0.36	11.11	0.56
	15.79	0.31	15.79	0.67
	20.00	0.31	20.00	0.81

to the interference of interfacial oxygen-containing functional groups on thermal transport. Although the addition of CNF also increased the interlayer spacing of MXene, a new bridging effect on thermal transport was formed, which made the out-of-plane thermal conductivity increase by 62%. This discovery provides a new idea for the preparation of MXene nTIM, which can modulate the thermal performance in a specific direction according to the properties of the fillers. It has a strong application prospect in the subsequent research on customized MXene composites.

Limitations of Study

In this study, the prepared MXene film contains a certain amount of L-Ascorbic acid sodium, and there is no method to completely remove it. At the same time, the MXene film has poor mechanical strength and is easily broken. In addition, the interaction of oxygen-containing functional groups in the prepared MXene@GO is currently difficult to characterize experimentally.

STAR★METHODS

Detailed methods are provided in the online version of this paper and include the following:

- KEY RESOURCES TABLE
- RESOURCE AVAILABILITY
  - Lead contact
  - Materials availability
  - Data and code availability
- METHOD DETAILS
  - Material preparation
  - Microstructure characterizations
  - Thermophysical property measurement

AUTHOR CONTRIBUTIONS

Conceptualization, L. Q., W. Y., and Y. F.; Methodology, Y. O., Y. B., and L. Q.; Investigation, Y. O., Y. B., and L. Q.; Writing, Y. O. and L. Q.; Funding Acquisition, L. Q.; Resource, L. Q. and W. Y.; Supervision, L. Q. and Y. F.

DECLARATION OF INTERESTS

The authors declare no competing interests.

REFERENCES

Badakhsh, A., Lee, Y.-M., Rhee, K.Y., Park, C.W., An, K.-H., and Kim, B.-J. (2019). Improvement of thermal, electrical and mechanical properties of composites using a synergistic network of length controlled-CNTs and graphene nanoplatelets. Compos. B Eng. 175, 107075. https://doi.org/10.1016/j.compositesb.2019.107075.

Borca-Tasciuc, T., Kumar, A.R., and Chen, G. (2001). Data reduction in 3ω method for thin-film thermal conductivity determination. Rev. Sci. Instrum. 72, 2139–2147. https://doi.org/10.1063/1.1353189.

Butler, S.Z., Hollen, S.M., Cao, L., Cui, Y., Gupta, J.A., Gutiérrez, H.R., Heinz, T.F., Hong, S.S., Huang, J., Ismach, A.F., et al. (2013). Progress, challenges, and opportunities in two-dimensional materials beyond graphene. ACS Nano 7, 2898–2926. https://doi.org/10.1021/nn400280c.

Cahill, D.G., and Pohl, R.O. (1987). Thermal conductivity of amorphous solids above the plateau. Phys. Rev. B Condens. Matter 35, 4067–4073. https://doi.org/10.1103/PhysRevB.35.4067.

Che, J., Jing, M., Liu, D., Wang, K., and Fu, Q. (2018). Largely enhanced thermal conductivity of HDPE/boron nitride/carbon nanotubes ternary composites via filler network-network synergy and orientation. Compos. A Appl. Sci. Manuf. 112, 32–39. https://doi.org/10.1016/j.compositesa.2018.05.016.

Che, J., Wu, K., Lin, Y., Wang, K., and Fu, Q. (2017). Largely improved thermal conductivity of HDPE/expanded graphite/carbon nanotubes ternary composites via filler network-network synergy. Compos. A Appl. Sci. Manuf. 99, 32–40. https://doi.org/10.1016/j.compositesa.2017.04.001.

Chen, L., Shi, X., Yu, N., Zhang, X., Du, X., and Lin, J. (2018). Measurement and analysis of thermal conductivity of Ti3C2Tx MXene films. Materials 11, E1701. https://doi.org/10.3390/ma11091701.

Gao, Q., Pan, Y., Zheng, G., Liu, C., Shen, C., and Liu, X. (2021). Flexible multilayered MXene/thermoplastic polyurethane films with excellent electromagnetic interference shielding, thermal conductivity, and management performances. Adv. Compos. Hybrid Mater. 4, 274–285. https://doi.org/10.1007/s42114-021-00221-4.

Ghidiu, M., Lukatskaya, M.R., Zhao, M.-Q., Gogotsi, Y., and Barsoum, M.W. (2014). Conductive two-dimensional titanium carbide 'clay' with high volumetric capacitance. Nature 516, 78–81. https://doi.org/10.1038/nature13970.

Gogotsi, Y., and Anasori, B. (2019). The rise of MXenes. ACS Nano 13, 8491–8494. https://doi.org/10.1021/acsnano.9b06394.

Hu, Q., Sun, D., Wu, Q., Wang, H., Wang, L., Liu, B., Zhou, A., and He, J. (2013). MXene: a new family of promising hydrogen storage medium. J. Phys. Chem. A 117, 14253–14260. https://doi.org/10.1021/jp409585v.

Jiao, E., Wu, K., Liu, Y., Lu, M., Hu, Z., Chen, B., Shi, J., and Lu, M. (2021a). Ultrarobust MXene-based laminated paper with excellent thermal conductivity and flame retardancy. Compos. A Appl. Sci. Manuf. 146, 106417. https://doi.org/10.1016/j.compositesa.2021.106417.

Jiao, E., Wu, K., Liu, Y., Lu, M., Zhang, H., Zheng, H., Xu, C.-a., Shi, J., and Lu, M. (2021b). Robust bioinspired MXene-based flexible films with excellent thermal conductivity and photothermal properties. Compos. A Appl. Sci. Manuf. 143, 106290. https://doi.org/10.1016/j.compositesa.2021.106290.

Lee, S.M., and Cahill, D.G. (1997). Heat transport in thin dielectric films. J. Appl. Phys. 81, 2590–2595. https://doi.org/10.1063/1.363923.

Liang, T., Shan, T.-R., Cheng, Y.-T., Devine, B.D., Noordhoek, M., Li, Y., Lu, Z., Phillpot, S.R., and Sinnott, S.B. (2013). Classical atomistic simulations of surfaces and heterogeneous interfaces with the charge-optimized many body (COMB) potentials. Mater. Sci. Eng. R Rep. 74, 255–279. https://doi.org/10.1016/j.mser.2013.07.001.

Lukatskaya, M.R., Mashtalir, O., Ren, C.E., Dall'Agnese, Y., Rozier, P., Taberna, P.L., Naguib, M., Simon, P., Barsoum, M.W., and Gogotsi, Y. (2013). Cation intercalation and high volumetric capacitance of two-dimensional titanium carbide. Science 341, 1502–1505. https://doi.org/10.1126/science.1241488.

Luo, S., Patole, S., Anwer, S., Li, B., Delclos, T., Gogotsi, O., Zahorodna, V., Balitskyi, V., and Liao, K. (2020). Tensile behaviors of Ti3C2Tx (MXene) films. Nanotechnology 31, 395704. https://doi.org/10.1088/1361-6528/ab94dd.

Mohseni Taromsari, S., Shi, H.H., Saadatnia, Z., Park, C.B., and Naguib, H.E. (2022). Design and development of ultra-sensitive, dynamically stable, multi-modal GnP@MXene nanohybrid electrospun strain sensors. Chem. Eng. J. 442, 136138. https://doi.org/10.1016/j.cej.2022.136138.

Murugan, N., Jerome, R., Preethika, M., Sundaramurthy, A., and Sundramoorthy, A.K. (2021). 2D-titanium carbide (MXene) based selective electrochemical sensor for simultaneous detection of ascorbic acid, dopamine and uric acid. J. Mater. Sci. Technol. 72, 122–131. https://doi.org/10.1016/j.jmst.2020.07.037.

Naguib, M., Kurtoglu, M., Presser, V., Lu, J., Niu, J., Heon, M., Hultman, L., Gogotsi, Y., and Barsoum, M.W. (2011). Two-dimensional nanocrystals produced by exfoliation of Ti3AlC2. Adv. Mater. 23, 4248–4253. https://doi.org/10.1002/adma.201102306.

Naguib, M., Mochalin, V.N., Barsoum, M.W., and Gogotsi, Y. (2014). 25th anniversary article: MXenes: a new family of two-dimensional materials. Adv. Mater. 26, 992–1005. https://doi.org/10.1002/adma.201304138.

Qiu, L., Ouyang, Y., Feng, Y., and Zhang, X. (2018). Note: thermal conductivity measurement of individual porous polyimide fibers using a modified wire-shape 3ω method. Rev. Sci. Instrum. 89, 096112. https://doi.org/10.1063/1.5052692.

Qiu, L., Ouyang, Y., Feng, Y., Zhang, X., Wang, X., and Wu, J. (2021a). Thermal barrier effect from internal pore channels on thickened aluminum nanofilm. Int. J. Therm. Sci. 162, 106781. https://doi.org/10.1016/j.ijthermalsci.2020.106781.

Qiu, L., Tang, D.W., Zheng, X.H., and Su, G.P. (2011). The freestanding sensor-based 3ω technique for measuring thermal conductivity of solids: principle and examination. Rev. Sci. Instrum. 82, 045106. https://doi.org/10.1063/1.3579495.

Qiu, L., Yan, K., Feng, Y., Liu, X., and Zhang, X. (2021b). Bionic hierarchical porous aluminum nitride ceramic composite phase change material with excellent heat transfer and storage performance. Compos. Commun. 27, 100892. https://doi.org/10.1016/j.coco.2021.100892.

Qiu, L., Zheng, X.H., Su, G.P., and Tang, D.W. (2013). Design and application of a freestanding sensor based on 3ω technique for thermal-conductivity measurement of solids, liquids, and nanopowders. Int. J. Thermophys. 34, 2261–2275. https://doi.org/10.1007/s10765-011-1075-y.

Sarycheva, A., and Gogotsi, Y. (2020). Raman spectroscopy analysis of the structure and surface chemistry of Ti3C2Tx MXene. Chem. Mater. 32, 3480–3488. https://doi.org/10.1021/acs.chemmater.0c00359.

Sun, Y., Chen, L., Cui, L., Zhang, Y., and Du, X. (2018). Molecular dynamics simulation of the effect of oxygen-containing functional groups on the thermal conductivity of reduced graphene oxide. Comput. Mater. Sci. 148, 176–183. https://doi.org/10.1016/j.commatsci.2018.02.037.

Wang, C., Lan, L., Liu, Y., and Tan, H. (2013). Functional group-guided variable frequency characteristics of a graphene resonator. RSC Adv. 3, 16095–16101. https://doi.org/10.1039/C3RA41683F.

Wang, J., Kang, H., Ma, H., Liu, Y., Wang, Y., and Fan, Z. (2021). Super-fast fabrication of MXene film through a combination of ion induced gelation and vacuum-assisted filtration. Eng. Sci. 15, 57–66. https://doi.org/10.30919/es8d446.

Wei, Z., Ni, Z., Bi, K., Chen, M., and Chen, Y. (2011). Interfacial thermal resistance in multilayer graphene structures. Phys. Lett. A 375, 1195–1199. https://doi.org/10.1016/j.physleta.2011.01.025.

Xiao, Y.-j., Wang, W.-y., Chen, X.-j., Lin, T., Zhang, Y.-t., Yang, J.-h., Wang, Y., and Zhou, Z.-w. (2016). Hybrid network structure and thermal conductive properties in poly(vinylidene fluoride) composites based on carbon nanotubes and graphene nanoplatelets. Compos. A Appl. Sci. Manuf. 90, 614–625. https://doi.org/10.1016/j.compositesa.2016.08.029.

Zhao, X., Vashisth, A., Prehn, E., Sun, W., Shah, S.A., Habib, T., Chen, Y., Tan, Z., Lutkenhaus, J.L., Radovic, M., and Green, M.J. (2019). Antioxidants unlock shelf-stable Ti3C2Tx (MXene) nanosheet dispersions. Matter 1, 513–526. https://doi.org/10.1016/j.matt.2019.05.020.

STAR★METHODS

KEY RESOURCES TABLE

REAGENT or RESOURCE	SOURCE	IDENTIFIER
Chemicals, peptides, and recombinant proteins		
Ti_3AlC_2 powder	11 technology Co., Ltd.	Purity: 98% Particle size: ∼74 μm CAS: 196506-01-1
HCl	Sinopharm Chemical Reagent Co., Ltd.	36.0–38.0% CAS: 7647-01-0
LiF	Sinopharm Chemical Reagent Co., Ltd.	≥98.0% CAS: 7789-24-4
L-Ascorbic acid sodium	Sinopharm Chemical Reagent Co., Ltd.	99.0% CAS: 134-03-2
Graphene oxide	Jiangsu XFNANO Materials Tech Co., Ltd	CAS: 7440-44-0
Carbon nanofibers dispersion	Guilin Qihong Technology Co., Ltd.	Industrial product
Software and algorithms		
MATLAB R2021b	MathWorks	https://ww2.mathworks.cn/products/matlab.html

RESOURCE AVAILABILITY

Lead contact

Further information and requests for resources and reagents should be directed to and will be fulfilled by the lead contact, Lin Qiu (qiulin@ustb.edu.cn).

Materials availability

This study did not generate new unique reagents.

Data and code availability

- All data reported in this paper will be shared by the lead contact upon request.

- This paper does not report original code.

- Any additional information required to reanalyze the data reported in this paper is available from the Lead contact upon request.

METHOD DETAILS

Material preparation

Pure MXene nanosheet and its composite films were prepared by the etching method (Ghidiu et al., 2014) (Figure 1). In brief, 1g LiF was added into 20 mL HCl and the mixture were stirred at room temperature for 30 min to make it fully dissolved. Then, 1g Ti_3AlC_2 was added into the mixture and the reaction occurred at 40°C for 24 h. Rinsing the MXene slurry with deionized water until PH = 6, and then sonicating the solution for 3 h in the N_2 atmosphere and vacuum filter to obtain the MXene powder. It is to be noted that the lateral size of the nanosheets in the powder can be controlled by the time of LiF corrosion and ultrasound during the etching process (Gogotsi and Anasori, 2019; Mohseni Taromsari et al., 2022). The dried MXene powder was prepared as MXene dispersion of 8 mg/mL. Finally, the L-Ascorbic acid sodium of 1 mg/mL was added and the MXene nanosheets were obtained by vacuum filtration (Zhao et al., 2019). As to the preparation of MXene@GO and MXene@CNF composite films, an additional 10 mL GO suspension and 1 mL CNF suspension was added in the last step. Four kinds of samples with different filler weight fraction (5.88 wt%, 11.11 wt

%, 15.79 wt%, and 20.00 wt%) were prepared separately to explore the filler effect on the thermophysical property of the MXene and its composite nanosheets.

Microstructure characterizations

Field emission transmission electron microscope (TEM, JEM-2200FS, Japan Electronics) was used to obtain microstructure information of the prepared MXene nanosheets. Scanning electron microscope (SEM, GeminiSEM500, Carl Zeiss) was used to characterize the surface and notch cross-section of the nanosheets. X-ray diffractometer (XRD, SMART LAB(9), Nippon Science Co. Ltd.) was used to measure the interlayer spacing information. Raman spectroscopy analyzer (Lab RAMHR Evolution, HORIBA Jobin Yvon S.A.S) was used to obtain the information about atomic vibrations and the structure of crystals.

Thermophysical property measurement

The home-made freestanding thermosensor-based 3ω method was used to measure the thermophysical properties of the nanosheets, which can avoid the difficulty of utilizing photolithography and chemical vapor deposition method to deposit metal thermosensors onto the MXene nanosheet for the conventional 3ω method. In brief, the freestanding thermosensor which encapsulates a metal strip with four pads by two pieces of polyimide films was sandwiched between two pieces of nanosheets and realize nondestructive measurement (Figure 2A). The two inner pads were used to measure the voltage, while the two outer ones were used for introducing electrical current. When an alternating current with angular frequency ω is passed through the strip, temperature fluctuations will be generated due to Joule effect, which will be transmitted to the nanosheets on both sides, thereby affecting the electrical resistance of the metal strip and generating a voltage signal with a frequency of 3ω. The test structure is symmetrical, that is from the center to the outside are metal strips, polyimide films, materials to be tested and highly thermal conductive substrates (stainless steel). Because the width of the metal strip (500 μm) is much larger than the thickness of the film (~50 μm), the heat flux of the system can be approximately transferred in the vertical direction of the film (Borca-Tasciuc et al., 2001). Figure 2B illustrates the electrical circuit for the implement of the freestanding sensor-based 3ω technique. The signal generator outputs alternating current signal with changeable frequencies, after amplified by a power amplification, the current signal goes through the thermosensor and the adjustable resistor box, and the voltage signals of them are captured by a lock-in amplifier. The diagram of the thermal resistance network method is shown in Figure 2C.

During the measurement, the frequency domain third harmonic voltages of the metal strip were measured and then the temperature rise of the strip was calculated by using:

$$\Delta T = \frac{2U_{3\omega}}{U_{1\omega} \times \alpha_{CR}}$$ (Equation 1)

where α_{CR} is the temperature coefficient of resistance of the metal strip. $U_{3\omega}$ and $U_{1\omega}$ are the third and first voltage amplitudes, respectively.

The difference between the temperature rise of the thermosensor measuring the structure with (T_{S+F}) and without (T_S) the MXene composite films is used to extract the out-of-plane thermal conductivity of the films according to:

$$T_{S+F} = T_S + \frac{pd_F}{2bl\kappa_F}$$ (Equation 2)

where subscript S denotes the substrate, subscript F denotes the film, p is the heating power, d is the film thickness, b is the half-width of the metal, l is the length of the metal strip, κ is the out-of-plane thermal conductivity (Lee and Cahill, 1997). The influence of the thermal properties of the polyimide film on the measurement can also be eliminated through the comparison between T_{S+F} and T_S.